Journal of Integrative Neuroscience

J. Integr. Neurosci. **2022**; 21(2): 063
https://doi.org/10.31083/j.jin2102063

Short Communication

Changes in subcortical white matter in the unaffected hemisphere following unilateral spontaneous intracerebral hemorrhage: a tract-based spatial statistics study

Young Hyeon Kwon[1], Sung Ho Jang[1,*]

[1]Department of Physical Medicine and Rehabilitation, College of Medicine, Yeungnam University, 705-717 Namku, Taegu, Republic of Korea
*Correspondence: strokerehab@hanmail.net (Sung Ho Jang)
Academic Editor: Filippo Brighina
Submitted: 5 May 2021 Revised: 1 June 2021 Accepted: 16 August 2021 Published: 23 March 2022

Abstract

We investigated changes in the subcortical white matter in the unaffected hemisphere in patients with unilateral intracerebral hemorrhage (ICH) by applying tract-based spatial statistics (TBSS) analysis. Twenty-four patients with ICH and 17 healthy control subjects were recruited for this study. Diffusion tensor imaging (DTI) data were obtained at least four weeks after ICH onset. TBSS analysis was performed using fractional anisotropy (FA) DTI data. We calculated mean FA values across the tract skeleton and within 27 regions of interest (ROIs) based on the observed intersections between the FA skeleton and the probabilistic Johns Hopkins University white matter atlases. The FA values of 27 ROIs in the unaffected hemisphere in the patient group were significantly lower than those of the control group ($p < 0.05$). In terms of a causal relationship between possible confounding factors (sex, age, lateralization [right], lesion volume), a negative correlation coefficient was observed in five ROIs (the tapetum, sagittal stratum, column and body of the fornix, posterior corona radiate, inferior cerebellar peduncle, superior cerebellar peduncle) in the regression analysis ($p < 0.05$). In the patient group, moderate negative correlations were detected between ICH volume and the FA values of two ROIs: the sagittal stratum, $r = –0.479$, $p < 0.05$; the tapetum, $r = –0.414$, $p < 0.05$. We detected extensive neural injury of the subcortical white matter in the unaffected hemisphere in patients with unilateral ICH. In addition, injury severities of neural structures located around the mid-sagittal line or periventricular areas were correlated with ICH volume.

Keywords: Unaffected hemisphere; White matter; Tract-based spatial statistics; Diffusion tensor imaging; Intracerebral hemorrhage

1. Introduction

Spontaneous intracerebral hemorrhage (ICH) is a subtype of stroke associated with high mortality and morbidity and accounts for about 15% of all deaths from stroke [1]. Neurological manifestations of ICH are usually associated with neural injury within the affected hemisphere; therefore, patients with ICH usually present with neurological manifestations on the contralateral side and related to motor and somatosensory functions [2]. However, hemiparetic patients with stroke can present functional deficits on the ipsilateral side [3–5]. Regarding the reported functional deficits of the ipsilateral side, several pathophysiological mechanisms have been suggested, including an interhemispheric imbalance in excitability, injury of the ipsilateral descending pathway, brain herniation, atrophy, and diaschisis (transneural depression) [4,6–10]. In addition, neural injury of the unaffected hemisphere via a biomechanical mechanism induced by barotrauma has been suggested [11,12]. However, the pathophysiological mechanisms of unaffected hemisphere injury following unilateral ICH have not been fully elucidated.

Diffusion tensor imaging (DTI) enables the assessment of white matter tracts using its ability to image water diffusion properties [13,14]. Among the various analytic methods used to assess DTI data, tract-based spatial statistics (TBSS) analysis is a widely used fully automated method to perform whole-brain tract DTI analysis based on the fractional anisotropy (FA) DTI parameter values [15]. The TBSS method is automated and a sensitive technique that can be used to perform precise voxel-based white matter analysis of several subjects [15]. The TBSS approach can compare whole-brain differences in neural tracts and extract a dispersion index for the white matter skeleton [15]. Therefore, TBSS analysis has been considered a reliable and appropriate method for obtaining information on the condition of and global changes in microstructures of the white matter of the brain [16]. A few studies have used TBSS to identify neural injuries of subcortical white matter in the affected hemisphere following unilateral ICH [17,18]. However, no studies have reported on changes in subcortical white matter in the unaffected hemisphere following unilateral ICH.

In this study, by using TBSS, we investigated changes in the subcortical white matter in the unaffected hemisphere in patients with unilateral ICH.

Table 1. Demographic data for the patient and control groups.

	Patient group (n = 24)	Control group (n = 17)
Age (years)	54.79 ± 9.67	50.94 ± 6.31
Sex, male/female	12/12	7/10
Hypoxemia/hypertension/diabetes mellitus/hematoma drainage OP	0/12/2/10	
Duration from ICH onset (months)	6.89 ± 3.02	
ICH hemisphere (Rt/Lt)	11/13	
Location of hematoma		
Basal ganglia	12	
Thalamus	1	
Putamen	6	
Corpus callosum	0	
Temporal parietal lobe	1	
Basal ganglia & thalamus	2	
Basal ganglia & thalamus & corpus callosum	2	
ICH volume	29.90 ± 23.88	
MMSE score	23.63 ± 5.44	

Values represent mean (± standard deviation); ICH, intracerebral hemorrhage; OP, operation; MMSE, Mini Mental State Examination.

2. Methods

2.1 Subjects

A total of 24 consecutive patients (12 men, 12 women; mean age 54.79 ± 9.67 years; range, 33–68 years) with unilateral ICH and 17 age- and sex-matched healthy control subjects (seven men, ten women; mean age 50.94 ± 6.31 years; range, 41–64 years) with no history of neurological/psychiatric disease or head trauma were recruited. The patients were recruited consecutively according to the following inclusion criteria: (1) first-ever stroke; (2) DTI data obtained at least four weeks after onset; (3) age at the time of ICH, 20~70 years; (4) ICH confined to a unilateral supratentorial area, which was verified by by a neuroradiologist using initial brain computed tomography (CT) results; (5) no subfalcine or transtentorial herniation on initial CT; (6) no intraventricular hemorrhage and hydrocephalus on initial brain CT or on T2-weighted images at DTI sequence of MRI images; (7) no previous history of neurologic/psychiatric disease. In the community, the control subjects were recruited consecutively according to the following inclusion criteria: (1) no previous history of neurologic/psychiatric disease, (2) no medical problem. The demographic data for the patient and control groups are summarized in Table 1. Significant difference in age or sex distribution was not detected between the patient and control groups ($p > 0.05$). This study was performed retrospectively, and the study protocol was allowed by the institutional review board of our university hospital. We explained for this study protocol and obtained the written informed consent from each patient and control subjects.

2.2 Diffusion tensor imaging

DTI data were acquired at an average of 6.89 ± 3.02 months after ICH onset by using a 6-channel head coil on a 1.5 T Philips Gyroscan Intera (Philips, Best, Netherlands) with single-shot echo-planar imaging. Sixty-five contiguous slices (reconstruction matrix = 192 × 192 matrix; acquisition matrix = 96 × 96; TE = 76 ms; field of view = 240 mm × 240 mm; TR = 10,726 ms, NEX = 1, slice gap = 0 mm, slice thickness = 2.5 mm, and b = 1000 s/mm^2) were acquired for each of the 32 noncollinear diffusion-sensitizing gradients. The Oxford Centre for Functional Magnetic Resonance Imaging of the Brain (FMRIB) Software Library was used for the analysis of DTI data. Affine multi-scale two-dimensional registration was used to correct head motion effects and image distortion due to eddy currents.

2.3 Tract-based spatial statistics

Functional MRI assessment tools included in the FMRIB Software Library (FSL) were used to execute the data analyses. A previously described method was used to generate the fractional anisotropy (FA) maps [15]. Voxel-wise statistical analysis of the FA data was performed using TBSS as implemented in FSL [16]. A nonlinear registration algorithm (www.doc.ic.ac.uk/~dr/software) was used to align the FA data for all subjects, obtained via FSL tools, to a template of average FA images (FMRIB-58) in Montreal Neurological Institute space. A mean FA image was produced and thinned to generate a mean FA skeleton representing the centers of all tracts common to the group members. A threshold was applied to a binarized mean FA skeleton at FA > 0.2 before the resulting data were fed into the voxel-wise statistical analysis. The aligned FA data for each subject were then projected onto the mean skeleton, and voxel-wise cross-subject statistics were procured to evaluate the differences between each group's FA values. The results were corrected for multiple comparisons

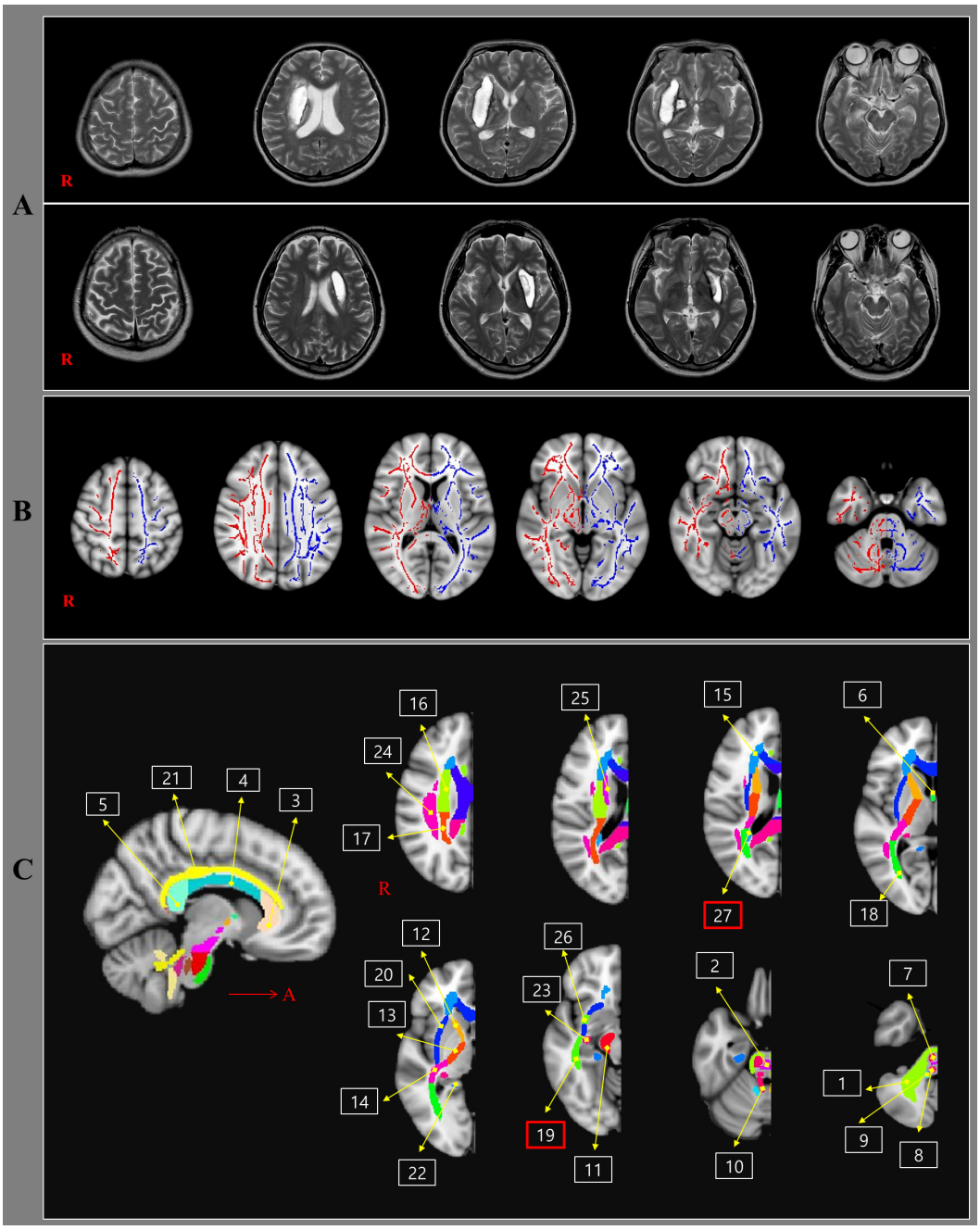

Fig. 1. Results of tract-based spatial statistics analyses comparing fractional anisotropy (FA) values of patient and control groups and the standard template of the Johns Hopkins University HU diffusion tensor imaging-based white matter atlases. (A) T2-weighted brain magnetic resonance images at the time of diffusion tensor image scanning in representative patients with unilateral right-intracerebral hemorrhage (41-year-old female) and left-intracerebral hemorrhage (50-year-old male). (B) The blue and red voxels represent areas with significantly lower mean FA values in the patient group than in the control group. (C) The 27 regions of interest (ROIs): (1) Middle cerebellar peduncle, (2) Pontine crossing tract, (3) Genu of corpus callosum, (4) Body of corpus callosum, (5) Splenium of corpus callosum, (6) Column and body of fornix, (7) Corticospinal tract, (8) Medial lemniscus R, (9) Inferior cerebellar peduncle, (10) Superior cerebellar peduncle, (11) Cerebral peduncle, (12) Anterior limb of internal capsule, (13) Posterior limb of internal capsule, (14) Retrolenticular part of internal capsule, (15) Anterior corona radiata, (16) Superior corona radiata, (17) Posterior corona radiata, (18) Posterior thalamic radiation (including the optic radiation), (19) Sagittal stratum (include inferior longitudinal fasciculus and inferior fronto-occipital fasciculus), (20) External capsule, (21) Cingulum (cingulate gyrus), (22) Cingulum, (23) Fornix (crus), (24) Superior longitudinal fasciculus, (25) Superior fronto-occipital fasciculus, (26) Uncinate fasciculus, and (27) Tapetum. Moderate negative correlations between intracerebral hemorrhage volume and the fractional anisotropy value (red rectangular boxes) are observed in the sagittal stratum (ROI 19) and the tapetum (ROI 27).

by controlling for the family-wise error rate after performing threshold-free cluster enhancement. For further exploration of the data, the voxels identified by TBSS analysis as showing substantial differences in each tract were selected, and the mean FA values for each subject were calculated. To summarize the FA data in a conventional neuroanatomical context and to identify relevant white matter tracts, mean FA values were calculated across the skeleton and within 48 regions of interest (ROIs); the ROIs were based on the intersections between the skeleton and the probabilistic Johns Hopkins University white matter atlases [15]. Differences in the FA values among 27 ROIs in the unaffected hemisphere were determined by subtracting the average FA value of the patient group from that of the control group. The obtained differences in the FA values were then arranged in descending order (Fig. 1).

2.4 Measurement of ICH volume

To determine the ICH volume in each patient, a simplified formula for calculation of the volume of an ellipsoid was applied by using initial brain CT data in the formula: ABC/2; where A = maximum length (cm), B = width perpendicular to A on the same head CT slice (cm), and C = the number of slices multiplied by the slice thickness (cm) [19].

2.5 Statistical analysis

Statistical analysis was performed by using SPSS 21.0 for Windows (SPSS, Chicago, IL, USA). The chi-squared test was used to assess differences in the sex composition of the groups. The Mann-Whitney U test was performed for the assessment of age differences and the determination of significant differences in FA values between the patient and control groups. Statistical significance was accepted for p values < 0.05. Multiple linear regressions was used to determine the association between possible confounding factors that could affect FA values of the 27 ROIs in the unaffected hemisphere. The possible confounding factors included in the regression model were sex, age, location of hematoma (lobar), lateralization (right: R), lesion volume, and hypertension. Multicollinearity was examined using the variance inflation factors (VIF) for each possible confounding factor. The independent variable with the value of tolerance less than the VIF more than ten, considered indicative of multicollinearity was excluded [20]. Statistical significance was determined as p-value < 0.05. In addition, The Spearman correlation coefficient was used to assess the correlations between ICH volume and FA values in the patient group and was considered significant when the p-value was <0.05. A correlation coefficient ≥ 0.60 indicated a strong correlation, a correlation coefficient between 0.40 and 0.59 indicated a moderate correlation, one between 0.20 and 0.39 indicated a weak correlation, and one <0.19 indicated a very weak correlation [21]. A minimum of 24 patients in each group was necessary to maintain a power of at least 80 percent when using the Mann-Whitney U test with a significance level of 0.05 to achieve an effect size of 0.8. The sample size calculation was performed with G-power 3.1.9.2 for Windows (University of Duesseldorf, Germany).

3. Results

The results of the voxel-wise comparison of the FA values of the patient and control groups are summarized in Table 2. The FA values of 27 ROIs in the unaffected hemisphere in the patient group were significantly lower than those of the control group ($p < 0.05$) (Fig. 1C).

In the patient and control groups, the results of multiple linear regression analysis of the possible confounding factors (sex, age) that contribute to the FA values of 27 ROIs of unaffected white matter are summarized in Table 2. Multicollinearity was not indicated when all possible confounding factors were included in multiple regression analysis for the FA of unaffected white matter (VIF >10). In multiple regression analysis for age and the FA values of the inferior cerebellar peduncle, superior longitudinal fasciculus, medial lemniscus, splenium of the corpus callosum, cerebral peduncle, uncinate fasciculus, posterior corona radiata, and middle cerebellar peduncle, the regression model showed statistical significance for the difference between the patient and control groups ($p < 0.05$). The inferior cerebellar peduncle, superior longitudinal fasciculus, medial lemniscus, splenium of corpus callosum, cerebral peduncle, uncinate fasciculus, posterior corona radiata and middle cerebellar peduncle were accepted in the model as associated with the variability in age (B = –0.002, –0.001, –0.002, –0.002, –0.001, –0.002, –0.001, –0.002, –0.001, respectively, $p < 0.05$). The multiple regression analysis of possible confounding factors (sex, age) and the FA of the cingulum hippocampus showed statistical significance for the difference between the patient and control groups ($p < 0.05$). The cingulum hippocampus was accepted in the model as explaining the variability in sex and age (B = –0.016, –0.001, respectively, $p < 0.05$). Except for the above results, the FA values of 17 ROIs in the unaffected hemisphere were not statistically accepted by the model as explaining the variability in sex and age ($p > 0.05$).

In the patient group, the results of multiple linear regression analysis for investigating the possible confounding factors (sex, age, location of hematoma [lobar], lateralization [R], lesion volume and hypertension) that contribute to the FA values of 27 ROIs in the unaffected hemisphere are summarized in **Supplementary Table 1** (see online supplemental materials file). Multicollinearity was not indicated when all possible confounding factors were included in multiple regression analysis for the FA values of 27 ROIs in the unaffected hemisphere (VIF >10). In multiple regression analysis for sex and FA values of two ROIs (the tapetum and inferior cerebellar peduncle), the regression model showed statistical significance ($p < 0.05$). The tape-

Table 2. Comparison of region-of-interest-based analysis of fractional anisotropy values between the patient and control groups and Multivariate Linear Regression Analysis to evaluate associations between possible confounding factors (sex, age) and fractional anisotropy values of 27 ROIs in the unaffected hemisphere in patient and control group.

	Patient group	Control group	*p*-value	Sex	Age	Adjusted R^2	*p*-value
Sagittal stratum (includes inferior longitudinal fasciculus and inferior fronto-occipital fasciculus	0.42 ± 0.03	0.46 ± 0.02	<0.00*	–0.016	–0.001	0.097	0.055
Tapetum	0.29 ± 0.05	0.32 ± 0.03	0.04*	–0.015	–0.001	0.023	0.241
Middle cerebellar peduncle	0.41 ± 0.02	0.46 ± 0.02	<0.00*	–0.015	–0.001**	0.124	0.031
Pontine crossing tract	0.40 ± 0.03	0.43 ± 0.02	<0.00*	–0.020	–0.001	0.073	0.090
Genu of corpus callosum	0.47 ± 0.03	0.53 ± 0.02	<0.00*	–0.010	–0.002	0.055	0.128
Body of corpus callosum	0.50 ± 0.03	0.56 ± 0.03	<0.00*	–0.019	–0.002	0.079	0.079
Splenium of corpus callosum	0.61 ± 0.04	0.67 ± 0.02	<0.00*	–0.024	–0.002**	0.150	0.017
Corticospinal tract	0.45 ± 0.04	0.49 ± 0.03	<0.00*	–0.009	–0.002	0.055	0.129
Medial lemniscus	0.51 ± 0.03	0.55 ± 0.03	<0.00*	–0.010	–0.002**	0.173	0.010
Inferior cerebellar peduncle	0.38 ± 0.03	0.42 ± 0.03	<0.00*	–0.017	–0.002**	0.333	<0.00
Superior cerebellar peduncle	0.46 ± 0.03	0.51 ± 0.02	<0.00*	–0.014	–0.001	0.082	0.074
Cerebral peduncle	0.56 ± 0.02	0.61 ± 0.02	<0.00*	–0.012	–0.002**	0.123	0.031
Anterior limb of internal capsule	0.44 ± 0.03	0.49 ± 0.02	<0.00*	–0.007	–0.002	0.086	0.068
Posterior limb of internal capsule	0.54 ± 0.02	0.59 ± 0.02	<0.00*	–0.014	–0.001**	0.136	0.023
Retrolenticular part of internal capsule	0.47 ± 0.02	0.52 ± 0.02	<0.00*	–0.017	–0.001	0.068	0.100
Anterior corona radiata	0.34 ± 0.03	0.40 ± 0.03	<0.00*	–0.003	–0.002	0.060	0.115
Superior corona radiata	0.39 ± 0.03	0.44 ± 0.02	<0.00*	–0.010	–0.001	0.067	0.102
Posterior corona radiata	0.38 ± 0.04	0.43 ± 0.02	<0.00*	–0.019	–0.002**	0.106	0.045
Posterior thalamic radiation (includes optic radiation)	0.48 ± 0.03	0.53 ± 0.03	<0.00*	–0.011	–0.002	0.087	0.067
External capsule	0.33 ± 0.02	0.37 ± 0.01	<0.00*	–0.007	–0.001	0.085	0.070
Cingulum cingulate gyrus	0.41 ± 0.03	0.46 ± 0.03	<0.00*	–0.006	–0.001	0.027	0.225
Cingulum hippocampus	0.33 ± 0.03	0.36 ± 0.03	<0.00*	–0.016**	–0.001**	0.176	0.010
Cres of fornix	0.40 ± 0.03	0.44 ± 0.04	<0.00*	–0.015	–0.002	0.079	0.079
Column and body of the fornix	0.30 ± 0.06	0.38 ± 0.07	<0.00*	–0.026	–0.002	0.011	0.308
Superior longitudinal fasciculus	0.40 ± 0.02	0.42 ± 0.01	<0.00*	–0.011	–0.001**	0.200	0.005
Superior fronto-occipital fasciculus	0.34 ± 0.04	0.41 ± 0.04	<0.00*	–0.008	–0.002	0.035	0.192
Uncinate fasciculus	0.39 ± 0.04	0.43 ± 0.03	<0.00*	–0.025**	–0.001**	0.115	0.037

Values represent mean (± standard deviation); *significant differences between the patient and control groups; **Significant result analyzed by multiple linear regression ($p < 0.05$).

tum and inferior cerebellar peduncle was accepted in the model as explaining the variability in sex (B = –0.021, –0.023, respectively, $p < 0.05$). In the multiple regression analysis of age and the inferior cerebellar peduncle, the regression model showed statistical significance of that relationship ($p < 0.05$). The inferior cerebellar peduncle was accepted in the model as explaining the variability in age (B = –0.002, $p < 0.05$). In multiple regression analyses lateralization [R] and the FA values of four ROIs (the tapetum, sagittal stratum, posterior corona radiata and superior cerebellar peduncle), the regression model showed statistical significance ($p < 0.05$). The FA values of four ROIs (the tapetum, sagittal stratum, posterior corona radiata and superior cerebellar peduncle) was accepted in the model as explaining the variability in lateralization [R] (B = –0.084, –0.034, –0.031, –0.033, respectively, $p < 0.05$). In multiple regression analysis for lesion volume and the sagittal stratum, the regression model showed statistical significance ($p < 0.05$). The sagittal stratum was accepted in the model as explaining the variability in sex (B = 0.000, $p < 0.05$). Except for the above results, the FA values of 22 ROIs in the unaffected hemisphere were not accepted in the model as explaining any of the variability in sex, age, location of hematoma (lobar), lateralization, lesion volume, and hypertension.

The correlations between the FA values of 27 ROIs and the ICH volume are summarized in **Supplementary Table 1** (see online supplemental materials file). Among the 27 ROIs, two ROIs showed a moderate negative correlation between the FA values of the unaffected hemisphere and ICH volume; those two ROIs are the sagittal stratum, $r = –0.479$, $p < 0.05$, and the tapetum, $r = –0.414$, $p < 0.05$ (Fig. 1C).

4. Discussion

In the current study, we used a TBSS-based approach to assess the state of the subcortical white matter of the unaffected hemisphere in patients with unilateral ICH and ob-

tained the following results. First, the FA values of 27 ROIs were lower in the patient group than those of the control group. Second, regarding the results of multiple linear regression analysis for a causal relationship between the possible confounding factors (sex, age, lateralization (R), lesion volume) and FA values of 27 ROIs in the unaffected hemisphere in the patient group, FA values of five ROIs showed a negative correlation coefficient (the tapetum: sex and lateralization (R); the sagittal stratum: lateralization (R) and lesion volume; the posterior corona radiata: lateralization (R); the inferior cerebellar peduncle: sex, age; the superior cerebellar peduncle: lateralization (R)). Third, in the patient group, moderately negative correlations in two ROIs (the sagittal stratum and the tapetum) among the 27 ROIs examined were observed between the FA values and the ICH volume.

Among the various DTI parameters, the FA value indicates the condition of white matter organization by suggeting integrity of white matter microstructures andthe degree of directionality, such as myelin, microtubules and axons [13]. A low FA value indicates a loss of white matter integrity, suggesting neural injury [13]. The FA values observed in 27 ROIs were lower in the patient group than in the control group, suggesting the presence of extensive neural injury to the subcortical white matter in the unaffected hemisphere of the ICH patients. Because we recruited patients whose ICH lesions were confined to a unilateral supratentorial area, this result suggests that the subcortical white matter of the so-called unaffected hemisphere can exhibit evidence of extensive injury.

In terms of the results of multiple linear regression analysis for a possible causal relationship between the confounding factors of sex, age, lateralization (R), and lesion volume and the FA values of 27 ROIs in the unaffected hemisphere in the patient group, the possible confounding factors were shown to have negative effects in five ROIs: The sex contributed to the FA values in the tapetum and inferior cerebellar peduncle; The age affected to the FA values in the inferior cerebellar peduncle; lateralization (R) influenced to the FA values in the tapetum, sagittal stratum, posterior corona radiata, superior cerebellar peduncle; lesion volume contributed to the FA values in the sagittal stratum.

In terms of the correlation between the FA values and ICH volume in the patient group, there were moderate negative correlations in two ROIs (the sagittal stratum and the tapetum). These two ROIs are located adjacent to the mid-sagittal line or periventricular areas. Thus, these correlations suggest increased injury severity in the neural structures located around the mid-sagittal line or periventricular areas. In 2001, Zazulia evaluated oxygen extraction fractions in 19 patients with ICH by using positron emission tomography [22]. They reported the oxygen extraction fraction was reduced rather than increased as a result of ischemia [22]. In 2009, the same author reported changes in the perihematomal cerebral glucose metabolic rate in 13 patients with ICH by using F-fluorodeoxyglucose positron emission tomography [23]. The author reported an increase in perihematomal glucose metabolism reflected by increased F-fluorodeoxyglucose uptake in the perihematomal region. In 2010, Power reviewed pathophysiological mechanisms for ICH and traumatic brain injuries. The author suggested that barotrauma from pressure waves propagated through intracranial regions is a common pathophysiological mechanism for ICH and traumatic brain injuries [12]. By contrast, many studies have demonstrated diaschisis of unaffected cerebellar following unilateral supratentorial stroke [24–28]. However, one study has reported diaschisis of the unaffected hemisphere following ICH [6]. In 1996, Tanaka *et al*. [6] found that patients with thalamic hemorrhage were more pronounced reduction of cerebral blood flow than those of patients with putaminal hemorrhages in both affected and unaffected hemisphere. They suggested that the reduction of cerebral blood flow may be secondary to metabolic depression due to diaschisis [6]. On that basis, we think that there might be two mechanisms to explain injury of the unaffected hemisphere. First, the extensive neural injuries of the subcortical white matter in the unaffected hemisphere following unilateral ICH might indicate that the axonal injuries are induced by internal barotrauma that cause the propagation waves immediately through the intracranial content, resulting in distal axotomy and demyelination [29]. Second, the diaschisis of unaffected hemisphere might be caused by decrease in metabolic activity and blood flow following unilateral ICH. Nevertheless, to the best of our knowledge, the current study is the first to investigate changes in the subcortical white matter in the unaffected hemisphere in patients with unilateral ICH.

However, some limitations of this study should be believed. First, the small number and limited age range of the subjects enrolled in the study limits the results. Second, we could not obtain relevant clinical data (e.g., modified Barthel Index, Fugl-Meyer Assessment, and modified Rankin Scale) that may be related to the neural injuries of the subcortical white matter in the unaffected hemisphere of the patient group because the study was performed retrospectively. Third, we could not assess the possibility of delayed expansion of ICH volume after onset. Therefore, further prospective studies that include larger numbers of subjects and detailed, long-term clinical data should be encouraged.

In conclusion, by performing TBSS analysis, we detected extensive neural injury of the subcortical white matter in the unaffected hemisphere in patients with unilateral ICH. In addition, injury severity in the neural structures located around the mid-sagittal line or periventricular areas was correlated with the ICH volume. Therefore, our results show the necessity of evaluating the unaffected hemisphere following a unilateral ICH. In addition, we suggest that TBSS-based results could be helpful when planning

neuro-rehabilitation because precise estimation of the extent and severity of a neural injury is necessary for establishing suitable therapeutic strategies and predicting prognosis.

Abbreviations

ICH, intracerebral hemorrhage; DTI, diffusion tensor imaging; TBSS, tract-based spatial statistics; FA, fractional anisotropy; CT, computed tomography; FSL, FMRIB Software Library; ROIs, regions of interest.

Author contributions

YHK and SHJ designed the research study. YHK performed the research. SHJ provided help and advice on the study. YHK analyzed the data. YHK and SHJ wrote the manuscript. All authors contributed to the editorial changes in the manuscript. All authors read and approved the final manuscript.

Ethics approval and consent to participate

All participants signed a written informed consent beforehand, which indicated they abided by the Helsinki Declaration, and all research activities were approved by the institutional review board of Yeungnam University Hospital (YUMC 2019-06-032).

Acknowledgment

Not applicable.

Funding

This work was supported by the National Research Foundation of Korea (NRF) grant funded by the Korean Government (MSIP) (No. 2021R1A2B5B01001386).

Conflict of interest

The authors declare no conflict of interest.

Supplementary material

Supplementary material associated with this article can be found, in the online version, at https://www.imrpress.com/journal/JIN/21/2/10.31083/j.jin2102063.

References

[1] Kase CS, Caplan LR. Intracerebral hemorrhage. Butterworth-Heinemann: Boston. 1994.

[2] Fewel ME, Thompson BG, Hoff JT. Spontaneous intracerebral hemorrhage: a review. Neurosurgical Focus. 2003; 15: E1.

[3] Brasil-Neto JP, de Lima AC. Sensory deficits in the unaffected hand of hemiparetic stroke patients. Cognitive and Behavioral Neurology. 2008; 21: 202–205.

[4] Noskin O, Krakauer JW, Lazar RM, Festa JR, Handy C, O'Brien KA, *et al*. Ipsilateral motor dysfunction from unilateral stroke: implications for the functional neuroanatomy of hemiparesis. Journal of Neurology, Neurosurgery, and Psychiatry. 2008; 79: 401–406.

[5] Bagnato S, Boccagni C, Boniforti F, Trinchera A, Guercio G, Letizia G, *et al*. Motor dysfunction of the "non-affected" lower limb: a kinematic comparative study between hemiparetic stroke and total knee prosthesized patients. Neurological Sciences. 2009; 30: 107–113.

[6] Tanaka A, Yoshinaga S, Nakayama Y, Kimura M, Tomonaga M. Cerebral blood flow and clinical outcome in patients with thalamic hemorrhages: a comparison with putaminal hemorrhages. Journal of the Neurological Sciences. 1996; 144: 191–197.

[7] Xi G, Keep RF, Hoff JT. Mechanisms of brain injury after intracerebral haemorrhage. The Lancet Neurology. 2006; 5: 53–63.

[8] Kalita J, Misra UK, Vajpeyee A, Phadke RV, Handique A, Salwani V. Brain herniations in patients with intracerebral hemorrhage. Acta Neurologica Scandinavica. 2009; 119: 254–260.

[9] Julkunen P, Könönen M, Määttä S, Tarkka IM, Hiekkala SH, Säisänen L, *et al*. Longitudinal study on modulated corticospinal excitability throughout recovery in supratentorial stroke. Neuroscience Letters. 2016; 617: 88–93.

[10] Kim J, Kim Y, Kim S, Kim S, Park J, Kim T, *et al*. Contralateral Hemispheric brain atrophy after primary Intracerebral hemorrhage. World Neurosurgery. 2017; 102: 56–64.

[11] Kummer TT, Magnoni S, MacDonald CL, Dikranian K, Milner E, Sorrell J, *et al*. Experimental subarachnoid haemorrhage results in multifocal axonal injury. Brain. 2015; 138: 2608–2618.

[12] Powers WJ. Intracerebral hemorrhage and head trauma: common effects and common mechanisms of injury. Stroke. 2010; 41: S107–S110.

[13] Mori S, Crain BJ, Chacko VP, van Zijl PC. Three-dimensional tracking of axonal projections in the brain by magnetic resonance imaging. Annals of Neurology. 1999; 45: 265–269.

[14] Basser PJ, Pajevic S, Pierpaoli C, Duda J, Aldroubi A. In vivo fiber tractography using DT-MRI data. Magnetic Resonance in Medicine. 2000; 44: 625–632.

[15] Smith SM, Jenkinson M, Johansen-Berg H, Rueckert D, Nichols TE, Mackay CE, *et al*. Tract-based spatial statistics: Voxelwise analysis of multi-subject diffusion data. NeuroImage. 2006; 31: 1487–1505.

[16] Anjari M, Srinivasan L, Allsop JM, Hajnal JV, Rutherford MA, Edwards AD, *et al*. Diffusion tensor imaging with tract-based spatial statistics reveals local white matter abnormalities in preterm infants. NeuroImage. 2007; 35: 1021–1027.

[17] Koyama T, Uchiyama Y, Domen K. Comparison of fractional anisotropy from tract-based spatial statistics with and without lesion masking in patients with intracerebral hemorrhage: a technical note. Journal of Stroke and Cerebrovascular Diseases. 2019; 28: 104376.

[18] Koyama T, Uchiyama Y, Domen K. Associations of diffusion-tensor fractional anisotropy and FIM outcome assessments after intracerebral hemorrhage. Journal of Stroke and Cerebrovascular Diseases. 2018; 27: 2869–2876.

[19] Kothari RU, Brott T, Broderick JP, Barsan WG, Sauerbeck LR, Zuccarello M, *et al*. The ABCs of measuring intracerebral hemorrhage volumes. Stroke. 1996; 27: 1304–1305.

[20] Miles J. Tolerance and variance inflation factor. Wiley StatsRef: Statistics Reference Online. 2014. Available at: https://doi.org/10.1002/9781118445112.stat06593 (Accessed: 18 March 2022).

[21] Cohen J. Statistical power analysis for the behavioral sciences. Psychological Bulletin. 1992; 112: 155–159.

[22] Zazulia AR, Diringer MN, Videen TO, Adams RE, Yundt K, Aiyagari V, *et al*. Hypoperfusion without ischemia surrounding acute intracerebral hemorrhage. Journal of Cerebral Blood Flow and Metabolism. 2001; 21: 804–810.

[23] Zazulia AR, Videen TO, Powers WJ. Transient Focal Increase in Perihematomal Glucose Metabolism after Acute Human Intracerebral Hemorrhage. Stroke. 2009; 40: 1638–1643.

[24] Lim JS, Ryu YH, Kim BM, Lee JD. Crossed cerebellar diaschisis due to intracranial hematoma in basal ganglia or thalamus. Journal of Nuclear Medicine. 1998; 39: 2044–2047.
[25] Fu J, Chen W, Wu G, Cheng J, Wang M, Zhuge Q, *et al*. Whole-brain 320-detector row dynamic volume CT perfusion detected crossed cerebellar diaschisis after spontaneous intracerebral hemorrhage. Neuroradiology. 2015; 57: 179–187.
[26] Noguchi T, Nishihara M, Egashira Y, Azama S, Hirai T, Kitano I, *et al*. Arterial spin-labeling MR imaging of cerebral hemorrhages. Neuroradiology. 2015; 57: 1135–1144.
[27] Yin L, Cheng S, Xiao J, Zhu Y, Bu S, Zhang X, *et al*. 3D pseudocontinuous arterial spin-labeling perfusion imaging detected crossed cerebellar diaschisis in acute, subacute and chronic intracerebral hemorrhage. Clinical Imaging. 2018; 50: 37–42.
[28] Sin DS, Kim MH, Park S, Joo MC, Kim MS. Crossed cerebellar diaschisis: risk factors and correlation to functional recovery in intracerebral hemorrhage. Annals of Rehabilitation Medicine. 2018; 42: 8–17.
[29] Mac Donald CL, Johnson AM, Cooper D, Nelson EC, Werner NJ, Shimony JS, *et al*. Detection of blast-related traumatic brain injury in U.S. military personnel. New England Journal of Medicine. 2011; 364: 2091–2100.